ELSEVIER

Applied Mathematical Modelling 22 (1998) 981–993

APPLIED MATHEMATICAL MODELLING

Modelling confined multi-material heat and mass flows using SPH

Paul W. Cleary [1]

CSIRO, Division of Mathematical and Information Sciences, Private Bag 10, Clayton South MDC, Clayton, Vic 3169, Australia

Received 1 July 1997; received in revised form 26 January 1998; accepted 26 February 1998

Abstract

Many applications in mineral and metal processing involve complex flows of multiple liquids and gases coupled with heat transfer. The motion of the surfaces of the liquids can involve sloshing, splashing and fragmentation. Substantially differing material properties are common. The flows are frequently complicated by other physical effects. Smoothed particle hydrodynamics (SPH) is a computational modelling technique that is ideally suited to such difficult flows. The Lagrangian framework means that momentum dominated flows and flows with complicated material interface behaviours are handled easily and naturally. To be able to model complex multi-physics flows, many aspects of SPH need to be explored. In this paper we describe developments that allow conductive and convective heat transfer to be modelled accurately for a sequence of idealised test problems.

Keywords: Smoothed particle hydrodynamics; Conduction; Natural convection; Particle boundaries

Nomenclature

m_b, r_b, v_b, n_b	mass, position, velocity and unit normal of particle b
X_{ab}	$X_a - X_b$ for any variable X
h	interpolation length
c_s	speed of sound
Δx	initial particle separation
η	small parameter
L, V	characteristic length and velocity scales
$P = P(\rho)$	pressure
T_0	reference temperature
U	internal energy
$T = U/c_v$	temperature
$\mathrm{Re} = \rho VL/\mu$	Reynolds number
$\mathrm{Ra} = \beta g \Delta T L^3/v\alpha$	Rayliegh number
$\mathrm{Pr} = v/\alpha$	Prandtl number
Nu	Nusselt number
$\alpha = k/\rho c_v$	thermal diffusivity

[1] Tel.: +61 3 9545 8000; fax: +61 3 9545 8080.

0307-904X/98/$ – see front matter
PII: S0307-904X(98)10031-8

β	coefficient of thermal expansion
μ	dynamic viscosity
$\nu = \mu/\rho$	kinematic viscosity
ρ	density
g	gravity
c_v	specific heat
k	conductivity

1. Overview of SPH

SPH is a Lagrangian method for solving partial differential equations. Essentially, the domain is discretised by approximating it by a series of roughly equi-spaced particles. They move (if fluid) and change their properties (e.g. temperature) in accordance with a set of ordinary differential equations derived from the original governing PDEs. It has been used highly successfully in astrophysical applications for two decades (see the review by Monaghan [1] for details and references). In recent years it has been developed as a method for incompressible isothermal enclosed flows [2]. The modelling of the boundary conditions represents a significant challenge that was not present in the earlier astrophysical calculations. Here we extend the method to heat conduction and then to coupled heat and mass flows.

SPH has a range of strong advantages in modelling industrial heat and mass flows:

- The Lagrangian framework allows momentum dominated flows to be easily handled.
- Complex free surface and material interface behaviour, including break-up into fragments, can be modelled naturally.
- Complicated physics such as multi-phase, realistic equations of state, compressibility, radiation, solidification and fracturing can be added with comparative ease.
- Is easily extendible to three dimensions.

Much work is still required before the potential of SPH for industrial CFD is realised. Some of these are addressed here.

2. The SPH method

The interpolated value of a function A at position r using the SPH methodology is:

$$A(r) = \sum_b m_b \frac{A_b}{\rho_b} W(r - r_b, h), \tag{1}$$

where the sum is over all particles b within a radius $2h$ of r. Here W is a spline based interpolation kernel of radius $2h$. It mimics the shape of a delta function but without the infinite tails. It is a C^2 function.

The gradient of the function A is given by

$$\nabla A(r) = \sum_b m_b \frac{A_b}{\rho_b} \nabla W(r - r_b, h). \tag{2}$$

Evaluating an interpolated product of two functions is given by the product of their interpolated values. The following SPH equations are the equations of motion of the particles. They are integrated using a predictor corrector scheme described in Monaghan [2].

2.1. Continuity equation

Our preferred form of SPH continuity equation is

$$\frac{\mathrm{d}\rho_a}{\mathrm{d}t} = \sum_b m_b(v_a - v_b)\nabla W_{ab}. \tag{3}$$

It is Galilean invariant (since the positions and velocities appear only as differences), has good numerical conservation properties and is not affected by free surfaces or density discontinuities [1,2]. We choose $c_s = 10$ V to ensure that the density variations are less than 1%, so that the fluid is effectively incompressible.

2.2. Momentum equation

A new form of the SPH momentum equation has been developed. It is

$$\frac{\mathrm{d}v_a}{\mathrm{d}t} = -\sum_b m_b \left[\left(\frac{P_b}{\rho_b^2} + \frac{P_a}{\rho_a^2} \right) - \frac{\xi}{\rho_a \rho_b} \frac{4\mu_a\mu_b}{(\mu_a + \mu_b)} \frac{v_{ab} \cdot r_{ab}}{r_{ab}^2 + \eta^2} \right] \nabla_a W_{ab} + g. \tag{4}$$

It has a more sophisticated viscous term than the original one given by Monaghan [2], involving an explicit viscosity which can be variable. It also ensures that stress is automatically continuous across material interfaces. This allows multiple materials with densities and viscosities varying by up to three orders of magnitude to be accurately simulated. Temperature dependent viscosities can also be used. Systematic tests of this new form using a Couette flow are described in Cleary [3]. Calibration against the known exact transient flow solution gives $\xi = 4.96333$. This value is independent of μ.

The timestep for the explicit integration is limited by the Courant condition modified for the presence of viscosity

$$\Delta t = \min_a \left\{ 0.5h / \left(c_s + \frac{2\xi\mu_a}{h\rho_a} \right) \right\}. \tag{5}$$

2.3. Energy equation

A new form of the SPH energy equation has been developed. It is

$$\frac{\mathrm{d}U_a}{\mathrm{d}t} = \sum_b \frac{4m_b}{\rho_a\rho_b} \frac{k_a k_b}{k_a + k_b} T_{ab} \frac{r_{ab} \cdot \nabla_a W_{ab}}{r_{ab}^2 + \eta^2}. \tag{6}$$

It has a more sophisticated conduction term than the original one given by Monaghan [1], involving an explicit conductivity which can be variable. It also ensures that heat flux is automatically continuous across material interfaces. This allows multiple materials with substantially different conductivities and specific heats to be accurately simulated. Temperature dependent conductivities can also be easily modelled.

The maximum timestep for the explicit integration of the energy equation is

$$\Delta t = \zeta \rho c_v h^2 / k. \tag{7}$$

Detailed stability tests were performed for a range of material parameters and showed that $\zeta = 0.1$ was sufficient to guarantee stability.

2.4. Equations of state

The pressure is given by the equation of state. For these simulations either

$$P = \rho \quad \text{or} \quad P = P_0\left[\left(\frac{\rho}{\rho_0}\right)^{\gamma} - 1\right] \tag{8}$$

is used, where $\gamma = 7$, P_0 is the magnitude of the pressure and ρ_0 is the reference density.

2.5. Physical boundaries

Solids are simulated in the same way as fluids in SPH. The essential difference is that the solid particles are fixed spatially and the continuity and momentum equations are not solved. Special provisions must be made at the edges of solids in order for the motion of the adjacent fluid to be modelled correctly. We use a potential based boundary force for the particles on the edges of solids. This very steep force field balances the fluid pressure and prevents the fluid particles from entering the solid. The basic formulation of these forces is described by Monaghan [2]. This has been modified in Monaghan [4] so that each boundary particle has a normal directed out into the fluid. This allows the boundary force at any location between boundary particles to be interpolated so as to provide a smooth force field. The boundary force produced by a line of boundary particles is then flat. This formulation allows the boundary particle density to be the same as in the solids and the fluids and eliminates the rippled force field that is produced by a line of point sources. Effectively any shape boundary can now be easily simulated.

2.6. Thermal boundaries

The default thermal boundary condition is adiabatic. Any SPH particles on a surface (whether solid or liquid) are effectively adiabatic, since there are no particles beyond with which they can exchange energy. This is an automatic natural boundary condition. Isothermal boundaries must be part of a solid and are identified by a tag. They are implemented simply by not changing the internal energy of these particles.

Heat fluxes through the isothermal boundaries can be calculated either directly, by estimating the temperature gradients, or by calculating the internal energy that needs to be added or removed from the boundary to maintain a constant temperature. In both cases the inward normal vector at each boundary particle location must be specified. At corners, the normal is chosen to have an orientation half way between the normals of the particles on either side.

The direct flux estimation involves evaluating the temperature gradient at each isothermal boundary particle location and summing

$$\Phi_a = \frac{1}{\rho_a}\sum_b 2m_b k_b T_{ab} r_{ab} \cdot n_a \frac{r_{ab} \cdot \nabla_a W_{ab}}{r_{ab}^2 + \eta^2}. \tag{9}$$

Alternatively, the heat flux can be estimated from the energy added/removed from the boundary particles in a timestep

$$\Phi_a = m_a \tau_a / \Delta x, \tag{10}$$

where τ_a is the gradient of thermal energy per unit mass, and summing over the boundary.

The thermal energy gradient depends on the smoothed density of the particles near the boundary. The present formulation of the SPH density does not give quite the right values near the boundaries. This does not affect the heat flows near adiabatic boundaries, but does affect the flow through isothermal ones. A density correction has been formulated that leads to very

accurate fluxes. This correction and a detailed description of the thermal boundary conditions is contained in Cleary and Monaghan [5].

2.7. An example configuration

Fig. 1 shows a typical set up of particles, physical and thermal boundaries and normals for natural convection in a square cavity. The particles are set up as a 20×20 grid. The outside boundary particles are stationary and form the solid container. The normals used in calculating the flat boundary force are shown by the lines starting on the outer particles and directed into the container. The normals of the corner particles are directed inwards at 45° angles and have the effect of rounding them slightly. The internal particles are fluid particles and are free to move during the simulation. The left and right boundaries are isothermal with temperatures T_c and T_h and are shown as dark grey. The top and bottom of the container are adiabatic. They and the fluid particles have temperature T_0 and are shown as light grey. There is no incompatibility in the multiple roles of the normals in the calculations of the heat fluxes and boundary forces.

3. Conduction

Several test problems follow that demonstrate the accuracy and versatility of the SPH approach for conduction problems. These and many other tests are described in detail in Cleary and Monaghan [5] and Cleary [6–8].

3.1. Discontinuous initial temperature

Conduction in a homogeneous slab (with $k=1$, $c_v=1$, $\rho=1000$) with discontinuous initial temperature is modelled using an 80×20 array of particles. Initially, the left half is cold ($T_l=0$) and the right half is hot ($T_r=1$).

The exact solution for this configuration is

$$T = T_c \begin{cases} \operatorname{Erfc}(x'/\alpha t) & \text{if } x < x_m, \\ 1 + \operatorname{Erf}(x'/\alpha t) & \text{if } x > x_m, \end{cases} \tag{11}$$

where $T_c=(T_r - T_l)/2$, x_m is the location of the initial temperature discontinuity and $x'=x - x_m$. Fig. 2 shows the temperature profiles across the slab early and late in the conduction process. The temperatures of the particles are shown as dots and the exact solution is given by the curve. Even

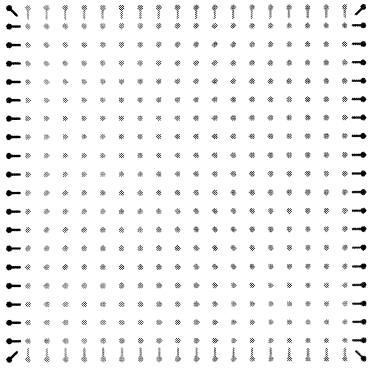

Fig. 1. Setup of particles and normals.

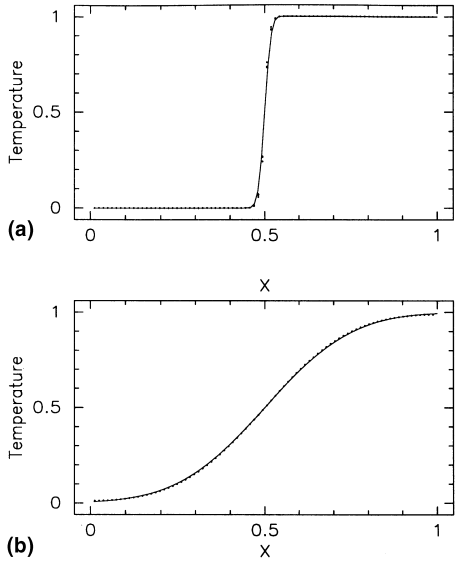

Fig. 2. Temperature profiles (a) early (b) late.

in the early stages when the temperature gradient is very high and there are only four particles to resolve it, the SPH solution is very accurate. Frame (b) shows that the SPH profile tracks the transient evolution very closely. The average errors at each time (even at this modest resolution) are less than 0.3%.

3.2. Discontinuous material properties

An essential requirement for industrial applications is to be able to model conduction across interfaces of materials with different thermal properties. Fig. 3 shows two examples using the

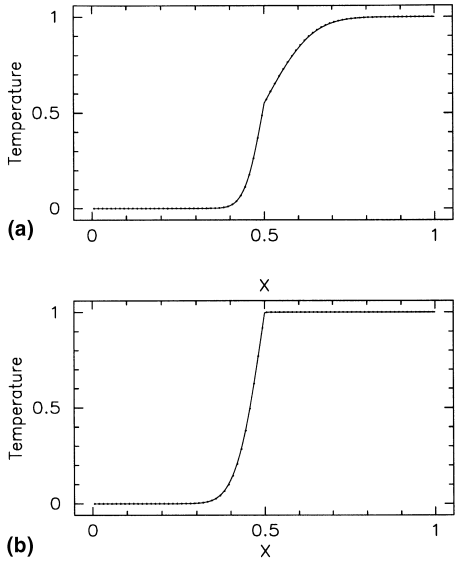

Fig. 3. Temperature profiles (a) $k_r/k_l = 3$ and $\rho_r/\rho_l = 0.5$ (b) air (left) and water (right).

same configuration, except now the materials on the left and right have different properties. $x = 0.5$ is now a material and temperature discontinuity. The points show the SPH temperatures and the curves show the corresponding exact solutions. The temperature profiles are shown at early times when the errors are largest. Frame (a) shows the case for modest differences in the density and conductivity and frame (b) shows the case for air and water. Both solutions are very accurate. This demonstrates that the flux conserving form of the energy equation 6, does ensure high accuracy even for density ratios as high as a thousand.

3.3. Temperature dependent k

Using the same geometry as above we model the conduction in a material with highly temperature dependent conductivity

$$k(T) = e^{4T}. \tag{12}$$

Fig. 4 shows the SPH solution (dots) and a high resolution finite element solution using *Fastflo* (curve) early on and at steady state. The profiles match extremely closely at all times with an average error of 0.1%. The steady SPH solution is also extremely close to the exact steady solution.

3.4. Sinusoidal temperature profile: 1D

Conduction is modelled in a homogeneous square slab (with $k = 1$, $c_v = 1$, $\rho = 10$) with an array of 40×40 particles and an initial sinusoidal temperature distribution. The exact solution is

$$T(x, y, t) = \sin\frac{\pi x'}{l} e^{-(\pi/l)^2 \alpha t}, \tag{13}$$

where l is the length of the block.

Fig. 5 shows the SPH and exact solutions midway through the simulation. They compare very well. This is typical of the accuracy throughout the simulation. The difference is largest near the

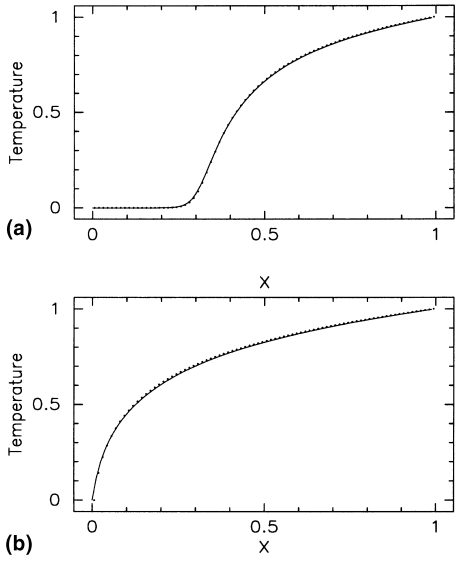

Fig. 4. Temperature profiles (a) early (b) late.

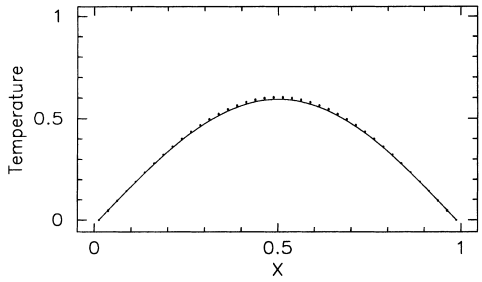

Fig. 5. Sinusoidal temperature profile.

center. This results from the heat transfer along the adiabatic top and bottom edges being marginally slower than through the middle of the slab.

Fig. 6 shows the exact flux (solid curve) and SPH fluxes through the isothermal sides as a function of time using the density correction. The fluxes are more accurate for the internal energy method of calculation (upper dotted curve) than for the direct method (lower dashed curve) with maximum errors of 1.4% and 3.1%, respectively. Without the density correction the errors are larger at 4.0% and 3.2%, respectively. In general, we have found that the internal energy method is the more accurate one and the correction improves the estimate by improving the accuracy of the contributions of the particles near the corners.

Fig. 7 shows the spatial variation of the flux along an isothermal edge at the same time as the temperature profile shown in Fig. 5. The point fluxes (dots) are very close to the exact value (solid line) except near the ends. The error at the ends is around 7% and results from the unphysical intersection of an adiabatic and an isothermal boundary. SPH, being a very physically based modelling method, smooths this discontinuity slightly. The errors at the ends are the dominant

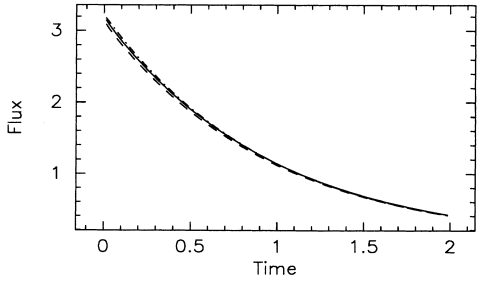

Fig. 6. Total heat flux absorbed by an isothermal edge.

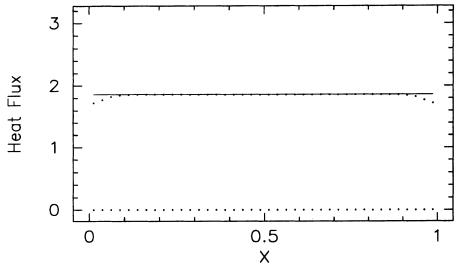

Fig. 7. Variation of heat flux along edge.

sources of error in the total heat fluxes. As the simulation resolution increases this error becomes decreasingly important and the total fluxes become more accurate.

3.5. Conduction in a disc: Correct setup

In previous tests, the edges of the particle lattice were aligned with the edge of the block. In general this is not the case. So how should we construct the boundaries in such cases? Consider heat conduction in a disc. The naive set up is to take all the particles on the lattice that lie within the circle and to tag the outermost ones as isothermal boundary particles. Such an approach actually produces very poor results. An unphysical temperature discontinuity forms just inside the isothermal particles as the boundary behaves partially isothermally and partially adiabatically. The problem is caused by the uneven spacing of the boundary particles. Nearby interior particles can effectively 'see' through the gaps between the isothermal boundary particles and behave partially adiabatically. The local boundary behaviour then depends on the precise details of the particle locations. This is exaggerated by the somewhat erratic directions of the boundary normals.

We have devised simple rules for setting up both isothermal and physical boundaries:

- Boundaries should be set up separately from the interior particles unless they align with the particle lattice.
- Boundary particles should be placed upon smoothly varying curves and should be equally spaced using the interior particle spacing Δx.
- The boundary normals should actually be perpendicular to the underlying boundary curve leading to smooth variations in the orientations of the normals.
- Interior particles within $\epsilon\Delta x$ of the boundary should be omitted.

Fig. 8 shows the set up for the disc using the rules above. The isothermal boundary particles are grey and form a circle. There are only 30 particles across this disc, but the heat conduction is very accurate.

Fig. 9(a) shows the temperature profile when the central temperature has declined by half. The SPH points are almost indistinguishable from the exact solution (the curve). The average error at each timestep is less than 0.5%. Tests indicate that the optimal value of ϵ is 0.42 and is good for

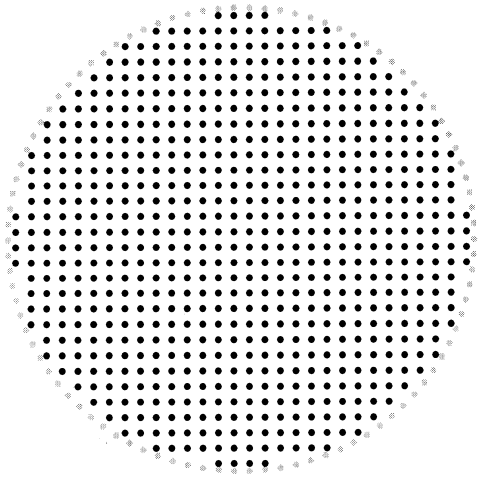

Fig. 8. Good set up for a disc.

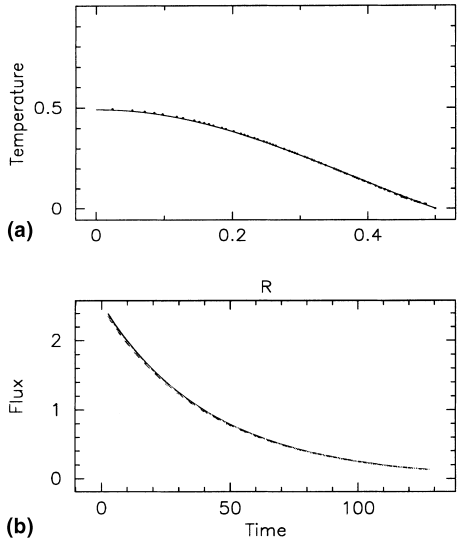

Fig. 9. (a) Temperature profile. (b) Flux.

most smaller values. If $\epsilon > 0.42$ the interior particles have insufficient thermal contact with the boundaries and adiabatic discontinuities ensue. Fig. 9(b) shows the time evolution of the total heat flux absorbed by the boundary. The results for both SPH flux calculation methods (dashed and dotted curves) are very close to the exact heat flux (solid curve). The heat flux is much more sensitive to errors than the temperature profile, so this demonstrates the high accuracy that can be achieved for SPH simulations of conduction, even with modest resolution, when using our rules for setting up the boundaries.

Similar tests were performed for heat transfer in a slab that was inclined to the lattice of particles. The errors were only marginally higher than for the case where the heat transfer is aligned with the lattice.

SPH particles in fluids do not remain in the initial lattice structure but move to a quasi-disordered state. The interior particles of the earlier slab were allowed to become disordered using a fluid simulation and were then fixed. The accuracy of heat conduction in this disordered solid was found to be comparable to that using an aligned lattice.

4. Natural convection

The Boussinesq approximation is easily implemented in SPH by replacing the body force g in Eq. (4) by $\beta g\ (T - T_0)$. We show two examples using air, which has $\mathrm{Pr} = 0.71$.

4.1. Flow in a square cavity

Natural convective flows in a differentially heated square cavity (shown in Fig. 10) are modelled for a range of Ra. Fig. 10 shows the isotherms for a range of Ra with SPH solutions on the left and finite element solutions from *Fastflo* on the right. The solutions are very close for $\mathrm{Ra} \leqslant 10^4$. For $\mathrm{Ra} = 10^5$ there are slight differences. The FE mesh had 60 nodes across the cavity and was graded geometrically towards the boundaries. The SPH solutions also used 60 particles across, except for $\mathrm{Ra} = 10^5$ which had 90 particles. The particles are equi-spaced so for the same

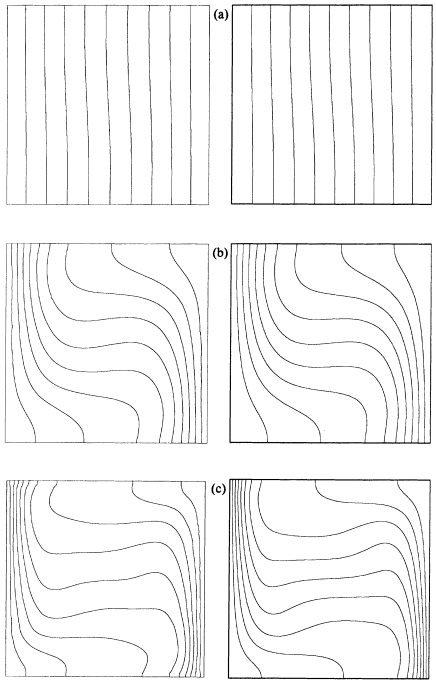

Fig. 10. (a) $\mathrm{Ra} = 100$, (b) $\mathrm{Ra} = 10^4$, (c) $\mathrm{Ra} = 10^5$.

particle/node numbers the SPH solution has less effective resolution in the important boundary layers. For low and moderate Ra this is sufficient to give excellent results. For higher Ra, the results deteriorate. To have the same resolution in the boundary layers (which determine the magnitude of the driving force for the convection and therefore the overall flow structure) we would require 150 particles across the cavity. This could be overcome by developing an SPH variant with a spatially dependent h. Overall, the SPH method seems to give equivalent results to that of finite elements when comparable resolution is used in the boundary layers.

Fig. 11 shows that the SPH and *Fastflo* Nu are within a few percent for low and moderate Ra. The flux is most sensitive to the adequacy of the resolution near the walls and so the SPH Nu begins to diverge for the higher Ra. Using more particles would improve these Nu predictions.

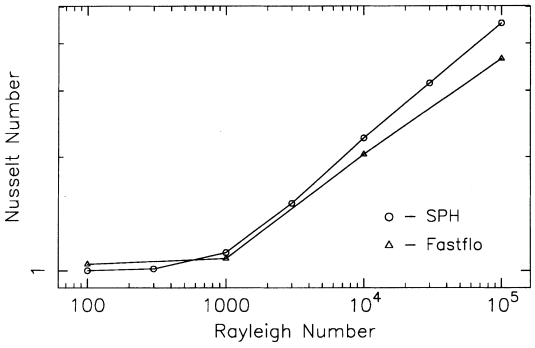

Fig. 11. Nu vs. Ra for the cavity.

4.2. Rayleigh–Benard convection

Prediction of instabilities is important so we simulate Rayleigh–Benard convection between a lower hot plate and an upper cold plate. We use periodic boundaries in the flow direction. Fig. 12 shows the steady flow for a control volume with aspect ratio 1.5 at $\mathrm{Ra} = 2.4 \times 10^4$. Frame (a) shows the particles and their velocities, shaded according to their temperature with light grey being hot. There are two very clearly defined recirculation cells, with the hot air rising in the left jet and cold air descending in the right one. The isotherms are shown in (b).

Conduction from the boundaries produces horizontal hot and cold boundary layers adjacent to the bottom and top surfaces, respectively. For Ra below a critical value $\mathrm{Ra_c}$, the conduction regime is stable and the final state is stationary with a constant vertical temperature gradient. For higher Ra, the flow is unstable and the isotherms buckle. This leads to a multi-cell convection pattern. The choice of control volume aspect ratio determines the wavenumber of the instability and therefore $\mathrm{Ra_c}$. For this case, SPH does predict the existence of an instability with a conduction regime below $\mathrm{Ra_c}$ and a convection one above, where our $\mathrm{Ra_c} \approx 2.15 \times 10^4$. We find $4000 < \mathrm{Ra_c} < 5000$ for the most unstable mode (aspect ratio 2).

5. Conclusions

For heat conduction:

- SPH can accurately predict high temperature gradients with only small numbers of particles. The full transient evolutions are very accurate. Furthermore, any errors decay faster than the heat diffuses making the method extremely robust.
- Heat flux conservation across interfaces with different materials properties on either side is built into the SPH energy equation and ensures accurate temperature profiles even when the variations are substantial.
- Transient heat conduction and steep temperature gradients resulting from strongly temperature dependent conductivities are well predicted.

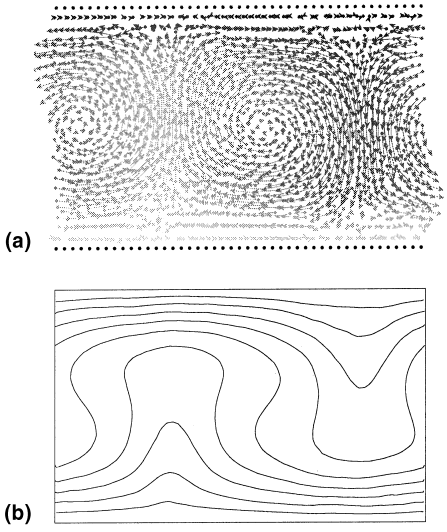

Fig. 12. (a) Rayleigh–Benard convection; (a) particles with velocity arrows; (b) isotherms.

- Rules were developed for construction of arbitrary shaped physical and isothermal boundaries that ensure accurate solutions.
- Heat conduction is as accurate when the heat transfer direction is not aligned with the particle lattice as when it is.
- Conduction has been accurately modelled in a wide variety of geometric shapes.
- Heat conduction in solids with disordered particles is also very accurate.

For natural convection:

- A simple Boussinesq body force term is easily implemented and gives good results.
- The accuracy of the results is dependent on the particle spacing in the boundary layers.
- SPH predictions of flow in a cavity are good when sufficient resolution is used in the boundary layers. Uniform particle spacing makes high Ra calculations expensive.
- Rayleigh–Benard instabilities are predicted by SPH. The wavenumber and Ra_c are determined by the width of the control volume leading to higher values than that for the most unstable mode occuring between infinite parallel plates.

References

[1] J.J. Monaghan, Smoothed particle hydrodynamics, Ann. Rev. Astron. Astro. 30 (1992) 543–571.
[2] J.J. Monaghan, Simulating free surface flows with SPH, J. Comp. Phys. 110 (1994) 399–406.
[3] P.W. Cleary, New implementation of viscosity: Tests with Couette flows, SPH Technical Note #8, CSIRO Division of Maths and Stats, Tech. Report DMS – C 96/32, 1996.
[4] J.J. Monaghan, Improved modelling of boundaries, SPH Tech. Note #2, CSIRO Div. of Maths and Stats, Tech. Report DMS – C 95/86, 1995.
[5] P.W. Cleary, J.J. Monaghan, Conduction IV: Isothermal boundary conditions and heat fluxes, SPH Tech. Note #7, CSIRO Div. of Maths and Stats, Tech. Report DMS - C 95/87, 1995.
[6] P.W. Cleary, Conduction II: 2 D heat conduction – accuracy, resolution and timesteps, SPH Technical Note #4, CSIRO Division of Maths and Stats, Tech. Report DMS – C 95/42, 1995.
[7] P.W. Cleary, Conduction III: 2 D heat conduction – example problems, SPH Technical Note #6, CSIRO Div. of Maths and Stats, Tech. Report DMS – C 95/43, 1995.
[8] P.W. Cleary, Conduction V: Heat conduction with disordered particles, SPH Technical Note #9, CSIRO Div. of Maths and Stats, Tech. Report DMS – C 95/96, 1996.